Chinese Journal of Aeronautics, (2016), xxx(xx): xxx–xxx

Chinese Society of Aeronautics and Astronautics
& Beihang University

Chinese Journal of Aeronautics

cja@buaa.edu.cn
www.sciencedirect.com

FULL LENGTH ARTICLE

Algorithm and experiments of six-dimensional force/torque dynamic measurements based on a Stewart platform

Wen Ke [a], **Du Fuzhou** [a,*], **Zhang Xianzhi** [b]

[a] *School of Mechanical Engineering and Automation, Beihang University, Beijing 100191, China*
[b] *School of Mechanical and Aerospace Engineering, Kingston University, London SW15 3DW, UK*

Received 31 March 2016; revised 26 April 2016; accepted 16 August 2016

KEYWORDS

Dynamic gravity compensation;
F/T-driven alignment;
Precision analysis;
P&O adjusting platform;
Six-dimensional F/T

Abstract Stewart platform (SP) is a promising choice for large component alignment, and interactive force measurements are a novel and significant approach for high-precision assemblies. The designed position and orientation (P&O) adjusting platform, based on an SP for force/torque-driven (F/T-driven) alignment, can dynamically measure interactive forces. This paper presents an analytical algorithm of measuring six-dimensional F/T based on the screw theory for accurate determination of external forces during alignment. Dynamic gravity deviations were taken into consideration and a compensation model was developed. The P&O number was optimized as well. Given the specific appearance of repeated six-dimensional F/T measurements, an approximate cone shape was used for spatial precision analysis. The magnitudes and directions of measured F/Ts can be evaluated by a set of standards, in terms of accuracy and repeatability. Experiments were also performed using a known applied load, and the proposed analytical algorithm was able to accurately predict the F/T. A comparison between precision analysis experiments with or without assembly fixtures was performed. Experimental results show that the measurement accuracy varies under different P&O sets and higher loads lead to poorer accuracy of dynamic gravity compensation. In addition, the preferable operation range has been discussed for high-precision assemblies with smaller deviations.

1. Introduction

The alignment of large-scale and complex components, such as airframes, satellites, and rockets, typically involves a large number of assembly fixtures, which control the position and orientation (P&O) of larger components in order to meet the accuracy requirement of the final assembly. Traditional fixed assembly fixtures can only be applied to the alignment of

* Corresponding author.
E-mail addresses: rongyu_wen@163.com (K. Wen), du_fuzhou@163.com (F. Du), X.Zhang@kingston.ac.uk (X. Zhang).

Peer review under responsibility of Editorial Committee of CJA.

Production and hosting by Elsevier

http://dx.doi.org/10.1016/j.cja.2016.10.015
1000-9361 © 2016 Production and hosting by Elsevier Ltd. on behalf of Chinese Society of Aeronautics and Astronautics.

one specific large component. Even a small change in the shape or structure of the large component will lead to redesigning and remanufacturing a new fixed assembly fixture. With the rapid development of the assembly technology toward becoming digital, more flexible and intelligent, digital flexible alignment systems have gained popularity for large component alignment, consisting of both software and hardware. The software includes a control system, a measurement system, a simulation system, and a calculation system. The hardware includes a P&O adjusting platform, digital measurement equipment, and an integrated control platform. The large components alignment process using a digital flexible alignment system has been transformed from the traditional process, based on manual fixtures and operations, to automatic alignment, which significantly improves aligning precision and efficiency.[1]

The P&O adjusting platform (such as the electronic mating alignment system, automated positioning systems based on POGOs, and parallel adjusting platforms), as a key section of the large component alignment, can automatically adjusts the P&O of large components.[2] In recent years, parallel robots have been widely used for P&O adjustments of large-scale component assembly, due to their outstanding advantages including high stiffness, high load capacity, fast motion, and high positioning accuracy.[3,4] Being the most frequently used structure of parallel robots, Stewart platforms (SPs) are suitable for machining and manufacturing,[5,6] surgical operations,[7] simulator designing,[8,9] flexible and precise assembly of aircraft sections,[10] spacecraft P&O adjustments,[11] and low-impact alignments.[12] An SP is composed of a moving platform and a base platform, which are connected with six stretchable limbs through spherical/universal joints. In the operation range, the 6-degrees-of-freedom (DOF) motion of the moving platform could be achieved by the motions of the six limbs as a whole.[13,14]

Currently, the main assembly strategy that is followed for a digital flexible alignment system is measurement aided assembly (MAA), which is based on geometrical control.[15] In order to direct and support the applications of advanced approaches in MAA for wing-fuselage alignment and realize the process integration and data fusion, a novel framework of measurement assisted assembly methodology has been proposed, based on key measurement.[16] Aiming to control the geometrical key characteristics and attain the best fit of P&O, which is a key feature in MAA, an optimization algorithm based on key characteristics for large component assembly has been proposed.[17] Using different measurement systems to measure the coordinates of points, the uncertainty of measurement results was analyzed from uncertainty contributions and setup procedures.[18,19] With the improvement of manufacturing and processing accuracy, a phenomenon that the accuracy of the measurement system is lower than that of assembly design takes place.[20] In this case, it will not only lead to an assembly failure, but also cause unexpected damages of components. Thus the measurement and control of the interaction force between components have great significance for the quality of the final product. Since six-dimensional force/torque (F/T) sensors can measure three-dimensional forces and three-dimensional torques with appropriate control techniques, they are commonly utilized to complete the force feedback loop control and high-precision assembly of components. The force measurement and control technology rely on two important parts: sensors and force control.

- Six-dimensional F/T sensors: Based on the elastomeric structure, six-dimensional F/T sensors can be divided into two groups: direct output type without coupling and indirect output type with coupling (including the SP structure). Structures of both types are fixed and unchangeable. Moreover, the isotropic configuration of a six-dimensional F/T sensor based on an SP, the task-oriented design method of a six-dimensional F/T sensor, and a six-dimensional F/T sensor have been introduced to complete peg-in-hole assembly tasks.[21,22] A six-beam sensor based on SP and the idea concept of "joint less" structure and beam sensors have been proposed to improve the precision and sensitivity in measuring a small F/T.[23] A six-dimensional heavy F/T sensor with high stiffness and good linearity based on SP has been presented.[24] Experimental results verified the feasibility and validity of the sensor by an established calibration platform. To summarize, six-dimensional F/T sensors have many types of forms and some advanced features. However, they are limited to the work environment and cannot be open-access designed for specific needs. Finally, they are very expensive.
- Force control techniques: A shape recognition algorithm based on a six-dimensional F/T sensor and a hole detection algorithm have been reported.[25] Experimental results showed that the two algorithms could complete the assembly of chamferless square peg-in-hole. The six-dimensional F/T sensor was employed to estimate the contact phases and design the assembling strategy to achieve force-guided robotic assembling.[26–28] The admittance characteristics for a force-guided robotic assembly and analytical derivations for different contact states were presented by Wiemer and Schimmels.[29] A modified control scheme for an SP with compensations for interaction force control and positional error recovery was introduced.[30] A novel strategy of the high-precision chamferless peg-hole insertion with a six-dimensional F/T sensor was introduced.[31] This strategy implemented the relation between a peg and a hole from the force sensor signal, and provided a wide range of initial conditions that affected the insertion. To summarize, a correct use of the interaction force can effectively achieve assembling. Finally, many control strategies have also been studied.

Following a literature review, traditional fixed assembly fixtures have been unable to meet the needs of large component alignment in a digital, flexible, and intelligent assembly process. On the contrary, the SP has gained popularity for its outstanding advantages in alignment of large-scale components. However, the measurement and control of the interaction forces between components should be considered. Therefore, a digital flexible alignment system with an SP based on six-dimensional F/T feedback and combined with force control techniques has been designed in this study. Due to the high manufacturing costs of six-dimensional F/T sensors and the required large size, they are not suitable for direct use in digital flexible alignment systems. Consequently, a P&O adjusting platform based on an SP and force sensors has been designed, which can adjust the P&O of a component and dynamically measure interactive forces. The platform uses six inexpensive

Please cite this article in press as: Wen K et al. Algorithm and experiments of six-dimensional force/torque dynamic measurements based on a Stewart platform, *Chin J Aeronaut* (2016), http://dx.doi.org/10.1016/j.cja.2016.10.015

force sensors placed in each limb to measure the forces of limbs and calculates the six-dimensional F/T based on measurement results. Moreover, combined with force control techniques, a precision analysis method of the six-dimensional F/T is proposed.

This paper takes into consideration multiple influential factors of the measurement accuracy of the interaction forces between components. Among the forces, gravity is of great research interest, and for the first time, this paper provides an analytical algorithm of a six-dimensional F/T with dynamic gravity compensation. The setup of the paper is as follows: Section 1 introduces the digital flexible assembly system and its significance, highlights the applications of the SP, and provides a new perspective and novel methods of large components alignment. Section 2 provides the analytical algorithm of a six-dimensional F/T, proposes a dynamic gravity compensation model based on the screw theory, and offers a parameter which is optimized through experiments. For the spatial precision analysis, Section 3 uses an approximate cone shape to evaluate the accuracy and repeatability of the six-dimensional F/T. In Section 4, using the designed P&O adjusting platform to verify the accuracy of the proposed algorithm and perform spatial precision experiments, relevant experimental data are analyzed and discussed. Section 5 concludes the paper and assesses the validity and limitations of the present algorithm and model.

2. Analytical algorithm of the six-dimensional F/T with dynamic gravity compensation

2.1. Overall research description

The overall study for calculating a six-dimensional F/T with dynamic gravity compensation can be depicted in the flowchart presented in Fig. 1. The P&O adjusting platform offers 6-DOF motion, due to the motions of six limbs as a whole, and the six-dimensional F/T is dynamically calculated by force sensors, which are placed in each limb to measure the forces of limbs. Moreover, due to the barycenter and gravity deviations of the large component, wrong calculation results will be derived. Thus, the dynamic gravity compensation is studied.

As shown in the left part of Fig. 1, a traditional six-dimensional F/T sensor is used to measure the six-dimensional F/T. The structural parameters of the sensor cannot be changed; hence, the measurement process is static. Since the lengths of the limbs remain unchanged after the initial setting, there are no sliding joints on the limbs. The six-dimensional F/T is calculated by measuring the forces of the limbs in o_1-$x_1y_1z_1$. As shown in the right part of Fig. 1, the P&O adjusting platform based on an SP is used to calculate the six-dimensional F/T. The length of the structural parameters is changed to adjust the P&O of the component; hence, the calculation process is dynamic. Moreover, the barycenter and gravity of the component must be dynamically compensated. Then, the six-dimensional F/T is calculated by measuring the forces of the limbs based on the dynamic gravity compensation in o_1-$x_1y_1z_1$.

2.2. Analytical algorithm of a six-dimensional F/T based on an SP

As presented in Fig. 2, the P&O adjusting platform based on an SP consists of a moving platform and a base platform, which are connected to each other with six limbs, adjustable in length through sliding joints. In the operation range, the 6-DOF motion of the moving platform could be achieved by the motions of the six limbs as a whole. Force sensors are placed in each limb to measure the force f_i applied to the limbs.

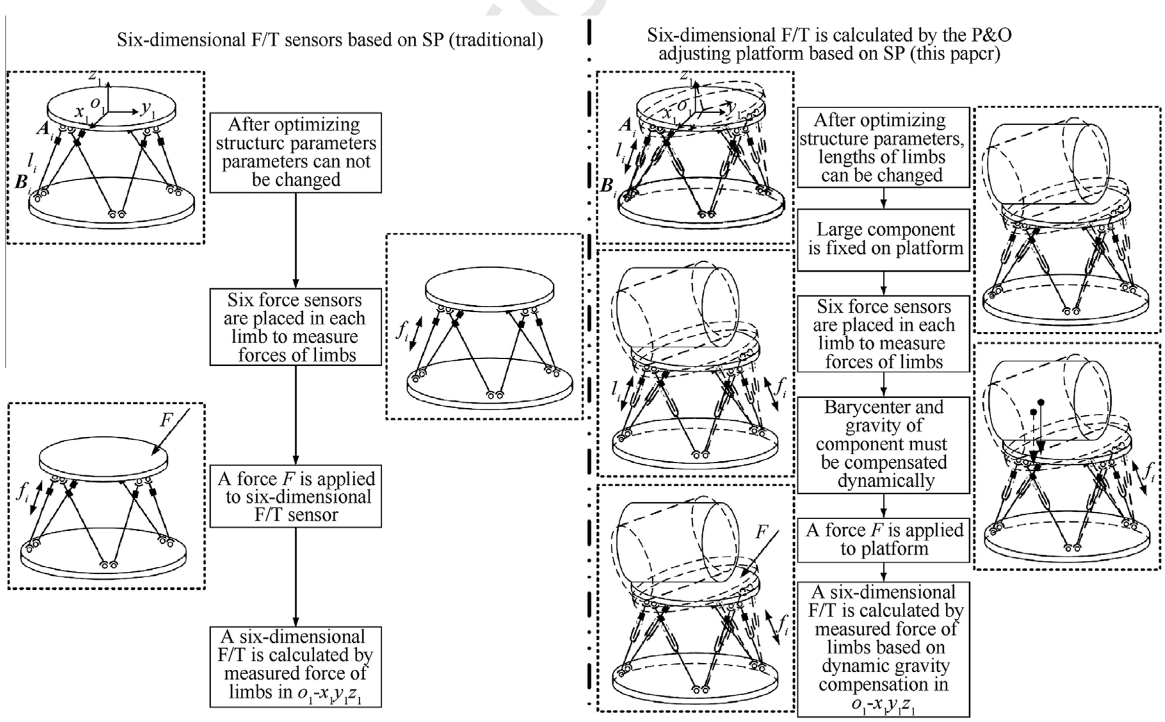

Fig. 1 Overview of overall study for calculating a six-dimensional F/T with dynamic gravity compensation.

Please cite this article in press as: Wen K et al. Algorithm and experiments of six-dimensional force/torque dynamic measurements based on a Stewart platform, *Chin J Aeronaut* (2016), http://dx.doi.org/10.1016/j.cja.2016.10.015

Encoders are used to measure the length l_i of the limbs ($i = 1, 2, \ldots, 6$). The Cartesian coordinate system of o_0-$x_0y_0z_0$ is located in the center of the top surface of the base platform, while the Cartesian coordinate system of o_1-$x_1y_1z_1$ is located in the center of the bottom surface of the moving platform. The centers of the spherical joints are denoted as $\boldsymbol{A}_i$ and $\boldsymbol{B}_i$.

The external load $[\boldsymbol{F}_s, \boldsymbol{M}_s]^T$ of the moving platform in o_1-$x_1y_1z_1$ could be calculated by the measured f_i and l_i. The six-dimensional F/T can be defined as follows:

$$[\boldsymbol{F}_s, \boldsymbol{M}_s]^T = g(f_i, l_i) \quad i = 1, 2, 3, 4, 5, 6 \tag{1}$$

where $[\boldsymbol{F}_s, \boldsymbol{M}_s]^T$ is the calculation results, and f_i and l_i are the measured forces and length data of the limbs, respectively.

Once the distance between $\boldsymbol{A}_i$ and $\boldsymbol{B}_i$ (limb length l_i) is set, the P&O parameters $\{x, y, z, \alpha, \beta, \gamma\}$ between o_1-$x_1y_1z_1$ and o_0-$x_0y_0z_0$ could be solved by the newton iteration method.[32] $\boldsymbol{S}_i$ and $\boldsymbol{S}_{0i}$ can be given by (as in Fig. 2):

$$\begin{cases} \boldsymbol{S}_i = \frac{\boldsymbol{A}_i - \boldsymbol{B}_i}{\|\boldsymbol{A}_i - \boldsymbol{B}_i\|} \\ \boldsymbol{S}_{0i} = \boldsymbol{A}_i \times \boldsymbol{S}_i \end{cases} \tag{5}$$

where $\boldsymbol{A}_i$ and $\boldsymbol{B}_i$ are the coordinates in o_1-$x_1y_1z_1$. However, in the actual calculation, $\boldsymbol{A}_i$ is the position vector from o_1-$x_1y_1z_1$ to the ith spherical joint and $\boldsymbol{B}_i$ is the position vector from o_0-$x_0y_0z_0$ to the ith universal joint. According to the P&O parameters $\{x, y, z, \alpha, \beta, \gamma\}$, Eq. (5) can be rewritten as follows:

$$\boldsymbol{S}_i = \frac{\boldsymbol{A}_i - \boldsymbol{R}^{-1}(\boldsymbol{B}_i - \boldsymbol{M})}{\|\boldsymbol{A}_i - \boldsymbol{R}^{-1}(\boldsymbol{B}_i - \boldsymbol{M})\|} \tag{6}$$

where

$$\boldsymbol{R} = \begin{bmatrix} \cos\alpha\cos\beta & \cos\alpha\sin\beta\sin\gamma - \sin\alpha\cos\gamma & \cos\alpha\sin\beta\cos\gamma + \sin\alpha\sin\gamma \\ \sin\alpha\cos\beta & \sin\alpha\sin\beta\sin\gamma + \cos\alpha\cos\beta & \sin\alpha\sin\beta\cos\gamma - \cos\alpha\sin\gamma \\ -\sin\beta & \cos\beta\sin\gamma & \cos\beta\cos\gamma \end{bmatrix} \tag{7}$$

$$\boldsymbol{M} = [x, y, z]^T \tag{8}$$

where $\boldsymbol{R}$ represents a rotation matrix and $\boldsymbol{M}$ represents a translation matrix.

Among the P&O parameters, x, y, and z are the displacements of o_1-$x_1y_1z_1$ with respect to o_0-$x_0y_0z_0$, and α, β, and γ are the rotation angles of o_1-$x_1y_1z_1$ with respect to o_0-$x_0y_0z_0$.

The force equilibrium equation could be defined in o_1-$x_1y_1z_1$ using the screw theory as follows:

$$\begin{bmatrix} \boldsymbol{F}_s \\ \boldsymbol{M}_s \end{bmatrix} = \sum_{i=1}^{6} f_i \$_{ii} \tag{2}$$

where $\$_{ii}$ is the unit screw along the ith leg, and could be obtained by the following:

$$\$_{ii} = \begin{bmatrix} \boldsymbol{S}_i \\ \boldsymbol{S}_{0i} \end{bmatrix} \tag{3}$$

where

$$\begin{cases} \boldsymbol{S}_i \boldsymbol{S}_i = 1 \\ \boldsymbol{S}_i \boldsymbol{S}_{0i} = 0 \end{cases} \tag{4}$$

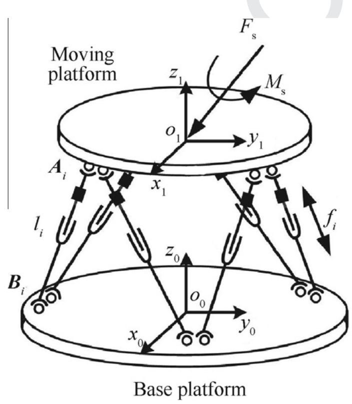

Fig. 2 Schematic diagram of a flexible fixture based on an SP for F/T-driven assembly.

Eq. (2) can be rewritten in the form of matrix equation as follows:

$$\boldsymbol{F} = \boldsymbol{G}\boldsymbol{f} \tag{9}$$

where

$$\boldsymbol{F} = [\boldsymbol{F}_s, \boldsymbol{M}_s]^T = [F_x, F_y, F_z, M_x, M_y, M_z]^T \tag{10}$$

$$\boldsymbol{f} = [f_1, f_2, f_3, f_4, f_5, f_6]^T \tag{11}$$

$$\begin{aligned} \boldsymbol{G} &= \begin{bmatrix} \boldsymbol{S}_1 & \boldsymbol{S}_2 & \boldsymbol{S}_3 & \boldsymbol{S}_4 & \boldsymbol{S}_5 & \boldsymbol{S}_6 \\ \boldsymbol{S}_{01} & \boldsymbol{S}_{02} & \boldsymbol{S}_{03} & \boldsymbol{S}_{04} & \boldsymbol{S}_{05} & \boldsymbol{S}_{06} \end{bmatrix} \\ &= \begin{bmatrix} \frac{\boldsymbol{A}_1 - \boldsymbol{R}^{-1}(\boldsymbol{B}_1 - \boldsymbol{M})}{\|\boldsymbol{A}_1 - \boldsymbol{R}^{-1}(\boldsymbol{B}_1 - \boldsymbol{M})\|} & \cdots & \frac{\boldsymbol{A}_6 - \boldsymbol{R}^{-1}(\boldsymbol{B}_6 - \boldsymbol{M})}{\|\boldsymbol{A}_6 - \boldsymbol{R}^{-1}(\boldsymbol{B}_6 - \boldsymbol{M})\|} \\ \boldsymbol{A}_1 \times \boldsymbol{S}_1 & & \boldsymbol{A}_6 \times \boldsymbol{S}_6 \end{bmatrix} \end{aligned} \tag{12}$$

Hence, the external load $[\boldsymbol{F}_s, \boldsymbol{M}_s]^T$ can be calculated by Eq. (1).

2.3. Dynamic gravity compensation

During the assembly process, the moving platform of the SP, assembly fixtures, and components are relatively heavy and bulky, so their barycenter and gravity deviations, which are caused by manufacturing errors and installation errors, will lead to wrong calculation results of the six-dimensional F/T. Additionally, during the measurements, the adjustable motions of the six limbs would also lead to the coordinate changes of barycenter in o_0-$x_0y_0z_0$ and the direction changes of gravity in o_1-$x_1y_1z_1$. To ensure the accuracy of the proposed analytical algorithm in Section 2.2, dynamic gravity compensation is needed.

2.3.1. Compensation model

The influential factors of the calculation results, which are the barycenter and gravity of the moving platform of the SP, assembly fixtures, and other components, cannot be ignored. This paper considers them as a rigid system. Eq. (9) can thus be rewritten as follows:

$$\boldsymbol{F}+\begin{bmatrix}\boldsymbol{S}_{\mathrm{G}}\\ \boldsymbol{S}_{0\mathrm{G}}\end{bmatrix}W=\boldsymbol{Gf} \tag{13}$$

where W is the dimensionless value of the gravity, so it is not a vector. $\boldsymbol{S}_{\mathrm{G}}$ is the gravity unit vector of the said rigid system, so it is a 3-column vector. $\boldsymbol{S}_{0\mathrm{G}}$ is the torque vector of $\boldsymbol{S}_{\mathrm{G}}$ with respect to o_1-$x_1y_1z_1$, so $\boldsymbol{S}_{0\mathrm{G}}$ is also a 3-column vector.

When the external load $F = 0$, the six-dimensional F/T is caused by the gravity of the rigid system (as in Fig. 3). The coordinate $\boldsymbol{C} = [x, y, z]^{\mathrm{T}}$ indicates the barycenter of the rigid system in o_1-$x_1y_1z_1$. The gravity is divided into forces, along the x_1-, y_1-, and z_1-axis (F_x, F_y, and F_z), and torques, about the x_1-, y_1-, and z_1-axis (M_x, M_y, and M_z), simultaneously. The relation between three-dimensional forces and three-dimensional torques is as follows:

$$\begin{bmatrix}M_x\\ M_y\\ M_z\end{bmatrix}=\begin{bmatrix}0 & -z & y\\ z & 0 & -x\\ -y & x & 0\end{bmatrix}\begin{bmatrix}F_x\\ F_y\\ F_z\end{bmatrix} \tag{14}$$

When the P&O of the moving platform changes, F_x, F_y, F_z, M_x, M_y, and M_z also change, while satisfying Eq. (14). According to the least square principle, $\boldsymbol{C}$ and W can be solved by the six-dimensional F/T under three different P&O sets. The accuracy of the compensation model can be improved by more measurements under different P&O sets. As an example, four measurements are performed here:

$$\begin{aligned}&\begin{bmatrix}M_{x1} & M_{x2} & M_{x3} & M_{x4}\\ M_{y1} & M_{y2} & M_{y3} & M_{y4}\\ M_{z1} & M_{z2} & M_{z3} & M_{z4}\end{bmatrix}\\ &=\begin{bmatrix}0 & -z & y\\ z & 0 & -x\\ -y & x & 0\end{bmatrix}\begin{bmatrix}F_{x1} & F_{x2} & F_{x3} & F_{x4}\\ F_{y1} & F_{y2} & F_{y3} & F_{y4}\\ F_{z1} & F_{z2} & F_{z3} & F_{z4}\end{bmatrix}\end{aligned} \tag{15}$$

The resolving process of $\boldsymbol{C}$ and W from Eq. (15) is similar to that of the generalized inverse matrix of $\begin{bmatrix}F_{x1} & F_{x2} & F_{x3} & F_{x4}\\ F_{y1} & F_{y2} & F_{y3} & F_{y4}\\ F_{z1} & F_{z2} & F_{z3} & F_{z4}\end{bmatrix}$. Since $\begin{bmatrix}F_{x1} & F_{x2} & F_{x3} & F_{x4}\\ F_{y1} & F_{y2} & F_{y3} & F_{y4}\\ F_{z1} & F_{z2} & F_{z3} & F_{z4}\end{bmatrix}$ is a matrix consisting of real numbers, its generalized inverse matrix is of unique existence. When the P&O changes, $\boldsymbol{C}$ and W of the rigid system do not differ in o_1-$x_1y_1z_1$, and the direction $\boldsymbol{S} = [0, 0, -1]^{\mathrm{T}}$ of the gravity does not vary in o_0-$x_0y_0z_0$, meaning:

$$\begin{cases}\boldsymbol{S}_{\mathrm{G}}=\dfrac{\boldsymbol{R}^{-1}\cdot\boldsymbol{S}}{\|\boldsymbol{R}^{-1}\cdot\boldsymbol{S}\|}\\ \boldsymbol{S}_{0\mathrm{G}}=\boldsymbol{C}\times\boldsymbol{S}_{\mathrm{G}}\end{cases} \tag{16}$$

which could serve for the solution of Eq. (13).

For the preparation of a six-dimensional F/T measurement, experiments without external loads were carried out first, and the measured F/Ts could be used for the calculations of $\boldsymbol{C}$ and W using Eq. (15), after which $\boldsymbol{C}$ was substituted into Eq. (16) for the vector $[\boldsymbol{S}_{\mathrm{G}}, \boldsymbol{S}_{0\mathrm{G}}]^{\mathrm{T}}$. Then, for an arbitrary external load, the six-dimensional F/T in o_1-$x_1y_1z_1$ could be obtained using Eq. (13) and the gravity of the rigid system could be dynamically compensated.

2.3.2. Parameter optimization

Without any external load, the measurement of the six-dimensional F/T should be equal to $[0, 0, 0, 0, 0, 0]^{\mathrm{T}}$ in o_1-$x_1y_1z_1$. However, the analytical algorithm is affected by the gravity of the rigid system, resulting in errors for actual measurements, which must be compensated. According to Eq. (15), the accuracy of the model could be more efficiently compensated and improved by measurements under additional different P&O sets. The determination of the P&O number is essential for efficient dynamic gravity compensation.

Following the instructions of the Monte Carlo method, n P&O sets were selected for experimental verification. Each set was repeated 200 times measurements, and the average values of the limb lengths and forces were obtained. A six-dimensional F/T can be calculated for each P&O and can be used for the calculations of $\boldsymbol{C}$ and W using Eq. (15). Substituting $\boldsymbol{C}$ into Eq. (16), for the vector $[\boldsymbol{S}_{\mathrm{G}}, \boldsymbol{S}_{0\mathrm{G}}]^{\mathrm{T}}$, the gravity of the rigid system can be dynamically compensated by using Eq. (13). The designed P&O adjusting platform applied in dynamic gravity compensation is presented in Fig. 4. The parameters of the P&O adjusting platform are listed in Table 1 and the graphical user interface (GUI) of data acquisition for dynamic gravity compensation is presented in Fig. 5.

For the determination of the proper selection of the P&O n number, another 50 P&O sets were selected, and the six-dimensional F/T after dynamic compensation could be

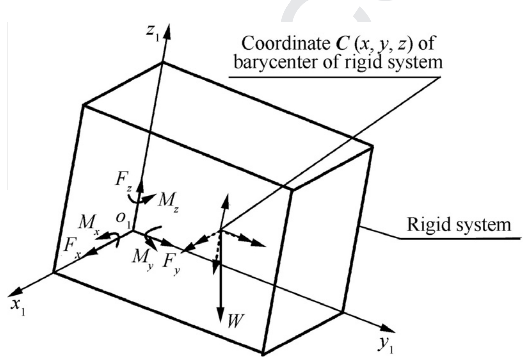

Fig. 3 Schematic diagram of the gravity of the rigid system in o_1-$x_1y_1z_1$.

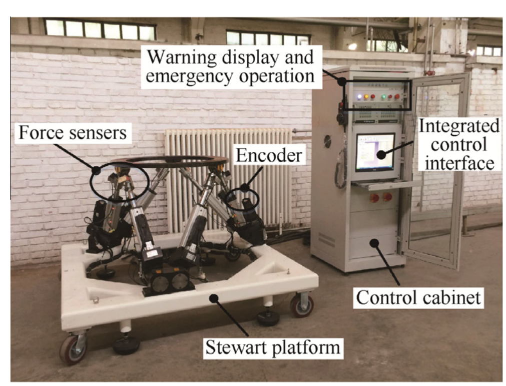

Fig. 4 Designed P&O adjusting platform applied in dynamic gravity compensation.

Please cite this article in press as: Wen K et al. Algorithm and experiments of six-dimensional force/torque dynamic measurements based on a Stewart platform, *Chin J Aeronaut* (2016), http://dx.doi.org/10.1016/j.cja.2016.10.015

Table 1 Parameters of the P&O adjusting platform.

Parameter name	Value
Moving range along x direction	± 50 mm
Moving range along y direction	± 50 mm
Moving range along z direction	± 50 mm
Rotation range along x direction	$\pm 5°$
Rotation range along y direction	$\pm 5°$
Rotation range along z direction	$\pm 5°$
Maximum load	800 kg
Accuracy	0.05 mm
Overall size	1.5 m $\times$ 1.5 m $\times$ 1 m

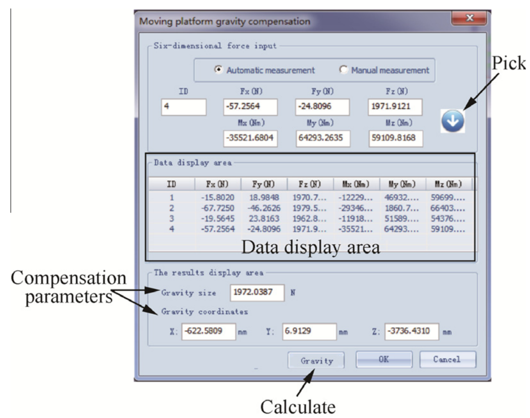

Fig. 5 GUI of data acquisition for dynamic gravity compensation.

obtained. The fluctuations between the compensated F/T and $[0, 0, 0, 0, 0, 0]^{\mathrm{T}}$ were calculated. For measurements repeating n times ($n = 3, 4, \ldots, 24$), the fluctuation range of the error is 3σ, where σ is the standard deviation. Experimental data are illustrated in Fig. 6.

From Fig. 6, it is noteworthy that the fluctuations after compensation were reduced with a higher n from the torques errors, indicating an enhanced compensation effect. The F_x, F_y, and F_z fluctuations show that the standard deviations vary along with n, yet within a small overall range, implying that the dynamic compensation of forces is of high stability and credibility. Regarding the M_x, M_y, and M_z fluctuations, the standard deviations decrease when n increases. In particular, the deviations of $n = 6$ have been significantly reduced compared to those of $n = 3$, indicating high converging rates of M_x and M_y.

For a stable and efficient compensation, the P&O number was selected to be 18 for the following experiments.

3. Spatial precision analysis of the six-dimensional F/T

The force control techniques take the magnitude and direction of the measured F/T into consideration; hence, by measuring the six-dimensional F/T, the magnitude and direction of the measured F/T could be illustrated as an approximate cone shape, as demonstrated in Fig. 7, which is utilized to evaluate the accuracy and repeatability of the six-dimensional F/T in the spatial precision analysis.

In an arbitrary coordinate system, six-dimensional F/T accuracy represents the deviation between an expected six-dimensional F/T and the average value of the measured F/T. The spatial precision standard in Fig. 7 can be described using the following parameters:

- Force direction accuracy A_{FD}: the angle between the expected direction and the central direction of measurements.
- Force magnitude accuracy A_{FM}: the difference between the expected magnitude and the average magnitude of measurements.

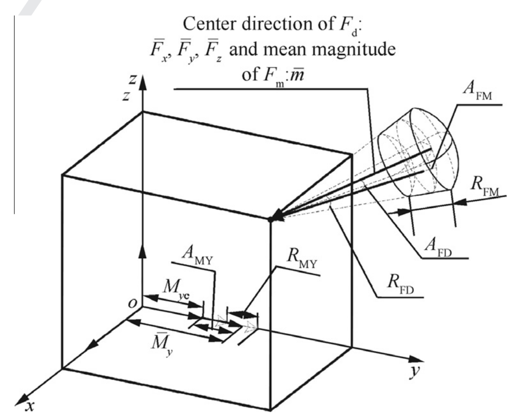

Fig. 7 Approximate cone shape for spatial precision analysis.

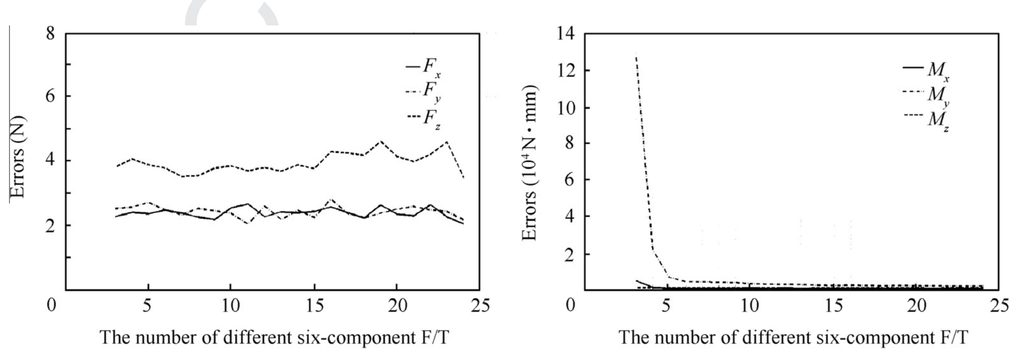

(a) Force errors (b) Torque errors

Fig. 6 Fluctuation analysis of the six-dimensional F/T after dynamic compensation.

- Torque accuracy A_{MX}, A_{MY}, A_{MZ}: the differences between the expected torques and the average torques of measurements (as A_{MY}, in Fig. 7).

In an arbitrary coordinate system, six-dimensional F/T repeatability stands for the variation in measurements for one expected six-dimensional F/T, which can be expressed by the following parameters:

- Force direction repeatability R_{FD}: half of the apex angle of the cone, formed by the measured directions.
- Force magnitude repeatability R_{FM}: spread of magnitude $\pm 3S_{\mathrm{FM}}$ about the mean value $\overline{m}$, where S_{FM} is the standard deviation.
- Torque repeatability R_{MX}, R_{MY}, R_{MZ}: spreads of torques $\pm 3S_{\mathrm{MX}}$, $\pm 3S_{\mathrm{MY}}$, $\pm 3S_{\mathrm{MZ}}$ regarding the mean values $\overline{M_x}$, $\overline{M_y}$, $\overline{M_z}$, where S_{MX}, S_{MY}, S_{MZ} are the standard deviations, respectively (as R_{MY} in Fig. 7).

3.1. Force direction and magnitude accuracy

Let $\overline{F_x}$, $\overline{F_y}$, $\overline{F_z}$ be the directional vectors of the center of the direction cluster for measurements that are repeated for n times, $F_{x\mathrm{c}}$, $F_{y\mathrm{c}}$, and $F_{z\mathrm{c}}$ the directional vectors of the expected force, and F_{xj}, F_{yj}, and F_{zj} the directional vectors of the jth measurement.

Then, the force direction accuracy A_{FD} and the force magnitude accuracy A_{FM} can be calculated as follows:

$$A_{\mathrm{FD}} = \frac{\sqrt{(\overline{F_x} - F_{x\mathrm{c}})^2 + (\overline{F_y} - F_{y\mathrm{c}})^2 + (\overline{F_z} - F_{z\mathrm{c}})^2}}{\sqrt{F_{x\mathrm{c}}^2 + F_{y\mathrm{c}}^2 + F_{z\mathrm{c}}^2}} \tag{17}$$

$$A_{\mathrm{FM}} = \sqrt{\overline{F_x}^2 + \overline{F_y}^2 + \overline{F_z}^2} - \sqrt{F_{x\mathrm{c}}^2 + F_{y\mathrm{c}}^2 + F_{z\mathrm{c}}^2} \tag{18}$$

where

$$\begin{cases} \overline{F_x} = \frac{1}{n}\sum_{j=1}^{n} F_{xj} \\ \overline{F_y} = \frac{1}{n}\sum_{j=1}^{n} F_{yj} \\ \overline{F_z} = \frac{1}{n}\sum_{j=1}^{n} F_{zj} \end{cases} \tag{19}$$

3.2. Torque accuracy

Let $\overline{M_x}$, $\overline{M_y}$, $\overline{M_z}$ be the mean values of the torques measurements that are repeated for n times, $M_{x\mathrm{c}}$, $M_{y\mathrm{c}}$, $M_{z\mathrm{c}}$ the expected torques, and M_{xj}, M_{yj}, M_{zj} the torques of the jth measurement, respectively. The torque accuracy A_{MX}, A_{MY}, A_{MZ} can be expressed as follows:

$$\begin{cases} A_{\mathrm{MX}} = \overline{M_x} - M_{x\mathrm{c}} \\ A_{\mathrm{MY}} = \overline{M_y} - M_{y\mathrm{c}} \\ A_{\mathrm{MZ}} = \overline{M_z} - M_{z\mathrm{c}} \end{cases} \tag{20}$$

where

$$\begin{cases} \overline{M_x} = \frac{1}{n}\sum_{j=1}^{n} M_{xj} \\ \overline{M_y} = \frac{1}{n}\sum_{j=1}^{n} M_{yj} \\ \overline{M_z} = \frac{1}{n}\sum_{j=1}^{n} M_{zj} \end{cases} \tag{21}$$

3.3. Torque accuracy

With the aforementioned $\overline{F_x}$, $\overline{F_y}$, $\overline{F_z}$ and F_{xj}, F_{yj}, F_{zj}, the force direction repeatability R_{FD} and the force magnitude repeatability R_{FM} can be defined as follows:

$$R_{\mathrm{FD}} = \overline{\theta_{\mathrm{d}}} + 3S_{\mathrm{FD}} \tag{22}$$

$$R_{\mathrm{FM}} = \pm 3S_{\mathrm{FM}} \tag{23}$$

where

$$\begin{cases} \overline{\theta_{\mathrm{d}}} = \frac{1}{n}\sum_{j=1}^{n} \theta_{\mathrm{d}j} \\ \theta_{\mathrm{d}j} = \frac{\sqrt{(F_{xj}-\overline{F_x})^2 + (F_{yj}-\overline{F_y})^2 + (F_{zj}-\overline{F_z})^2}}{\sqrt{\overline{F_x}^2 + \overline{F_y}^2 + \overline{F_z}^2}} \\ S_{\mathrm{FD}} = \sqrt{\frac{1}{n-1}\sum_{j=1}^{n}(\theta_{\mathrm{d}j} - \overline{\theta_{\mathrm{d}}})^2} \\ S_{\mathrm{FM}} = \sqrt{\frac{1}{n-1}\sum_{j=1}^{n}\left(\sqrt{F_{xj}^2 + F_{yj}^2 + F_{zj}^2} - \sqrt{\overline{F_x}^2 + \overline{F_y}^2 + \overline{F_z}^2}\right)^2} \end{cases} \tag{24}$$

3.4. Torque accuracy

The torque repeatability R_{MX}, R_{MY}, R_{MZ} can be obtained by the following:

$$\begin{cases} R_{\mathrm{MX}} = \pm 3S_{\mathrm{MX}} = \pm 3\sqrt{\frac{1}{n-1}\sum_{j=1}^{n}(M_{xj} - \overline{M_x})^2} \\ R_{\mathrm{MY}} = \pm 3S_{\mathrm{MY}} = \pm 3\sqrt{\frac{1}{n-1}\sum_{j=1}^{n}(M_{yj} - \overline{M_y})^2} \\ R_{\mathrm{MZ}} = \pm 3S_{\mathrm{MZ}} = \pm 3\sqrt{\frac{1}{n-1}\sum_{j=1}^{n}(M_{zj} - \overline{M_z})^2} \end{cases} \tag{25}$$

4. Experimental results and discussion

4.1. Measurement of a known applied load

The designed P&O adjusting platform is presented in Fig. 4. To measure a known applied load, three steps have been followed in this paper. Firstly, a known six-dimensional F/T is applied to the P&O adjusting platform. The through-hole of the moving platform is used to hang the known load. In this paper, the coordinates of the through-hole are $[302.874, -175.192, 89.64]^{\mathrm{T}}$ in o_1-$x_1y_1z_1$, the known load is 15 kg, and the P&O is $\{0, 0, 0, 0, 0, 0\}$. Hence, the value of the six-dimensional F/T can be calculated by the proposed algorithm and be expressed as $[0, 0, -150, 26278.8, 45431.1, 0]^{\mathrm{T}}$ in o_1-$x_1y_1z_1$. Secondly, measuring the load 1000 times repeatedly, under dynamic gravity compensation, 1000 measurement results of the six-dimensional F/T can be obtained.

Please cite this article in press as: Wen K et al. Algorithm and experiments of six-dimensional force/torque dynamic measurements based on a Stewart platform, *Chin J Aeronaut* (2016), http://dx.doi.org/10.1016/j.cja.2016.10.015

Thirdly, the analytical predictions of the proposed algorithm are presented in Fig. 8. The accuracy and repeatability analyses are listed in Tables 2 and 3, respectively. Finally, additional 1000 measurement results of the six-dimensional F/T are used to verify the validity of the calculation results and conclusions can be acquired.

From Fig. 8, it is noteworthy that the proposed algorithm could accurately predict the forces and torques in consistency with the theoretical values. Together with the experimental data, the force direction accuracy A_{FD} is 0.003 rad and the force direction repeatability R_{FD} is $0.107 + 3 \times 0.048$ rad; the force magnitude accuracy A_{FM} is 0.329 N and the force magnitude repeatability R_{FM} is $\pm 3 \times 13.668$ N, which are ideal for the six-dimensional F/T measurements. Comparisons between Tables 2 and 3 could also lead to the conclusion that the accuracy and repeatability of force were improved, compared to those of torque, which is attributed to the difference in their physical properties. For the force measurements, the errors could offset due to their directions. However, for the torque measurements, the deviations would be amplified by the arm of force for experiments.

Measuring the load 1000 times repeatedly, under dynamic gravity compensation, 1000 measurements of the six-dimensional F/T are all within the scopes of Tables 2 and 3. Thus, the method of the spatial precision analysis is considered as correct.

4.2. Precision analysis of measuring the six-dimensional F/T

Dynamic gravity compensation is critical for high-precision assembly and serves as an efficient tool for preliminary calibration before actual measurements. The designed P&O adjusting platform based on an SP for F/T-driven alignment can adjust the P&O, and dynamically measure interactive forces. However, the measurement accuracy of the six-dimensional F/T is different under different P&O sets and the accuracy of dynamic gravity compensation presented in this paper could be affected by the gravity of the rigid system. In this section, experiments were carried out with the P&O adjusting platform and spatial accuracy analyses were provided. Different P&O parameters $\{x, y, z, \alpha, \beta, \gamma\}$ were discussed. A comparison between compensations with or without assembly fixtures was also presented.

The P&O number $n = 18$ has been selected based on Section 2.2. Under limb length variations, 18 groups of six-dimensional F/T were obtained, and the barycenter $\boldsymbol{C}$ and the gravity value W could be determined.

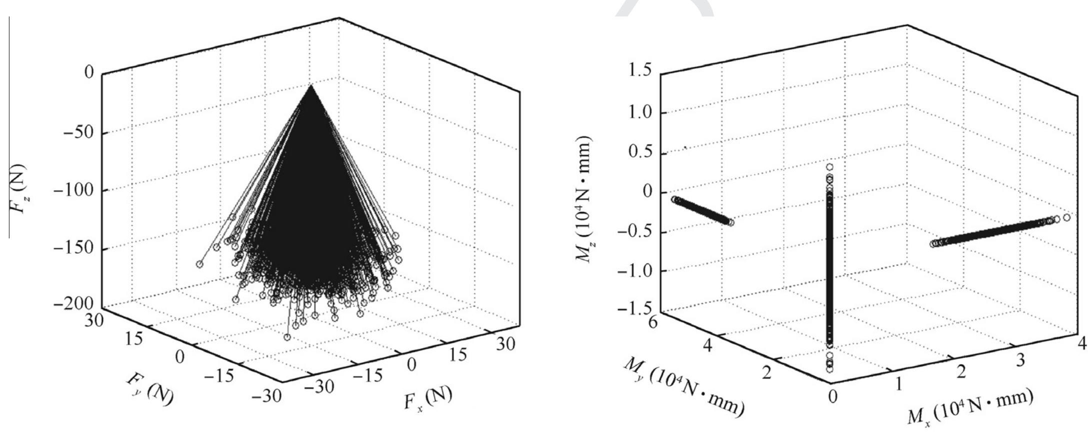

(a) Forces (b) Torques

Fig. 8 Measurement results of a known applied load.

Table 3 Repeatability analysis of the six-dimensional F/T.

Item	R_{FD} (rad)	R_{FM} (N)	R_{MX} (N·mm)	R_{MY} (N·mm)	R_{MZ} (N·mm)
Value	$0.107 + 3 \times 0.048$	$\pm 3 \times 13.668$	$\pm 3 \times 3255.6$	$\pm 3 \times 3305$	$\pm 3 \times 3742.7$

Table 2 Accuracy analysis of the six-dimensional F/T.

Item	A_{FD} (rad)	A_{FM} (N)	A_{MX} (N·mm)	A_{MY} (N·mm)	A_{MZ} (N·mm)
Value	0.003	0.329	9.689	−93.488	−94.210

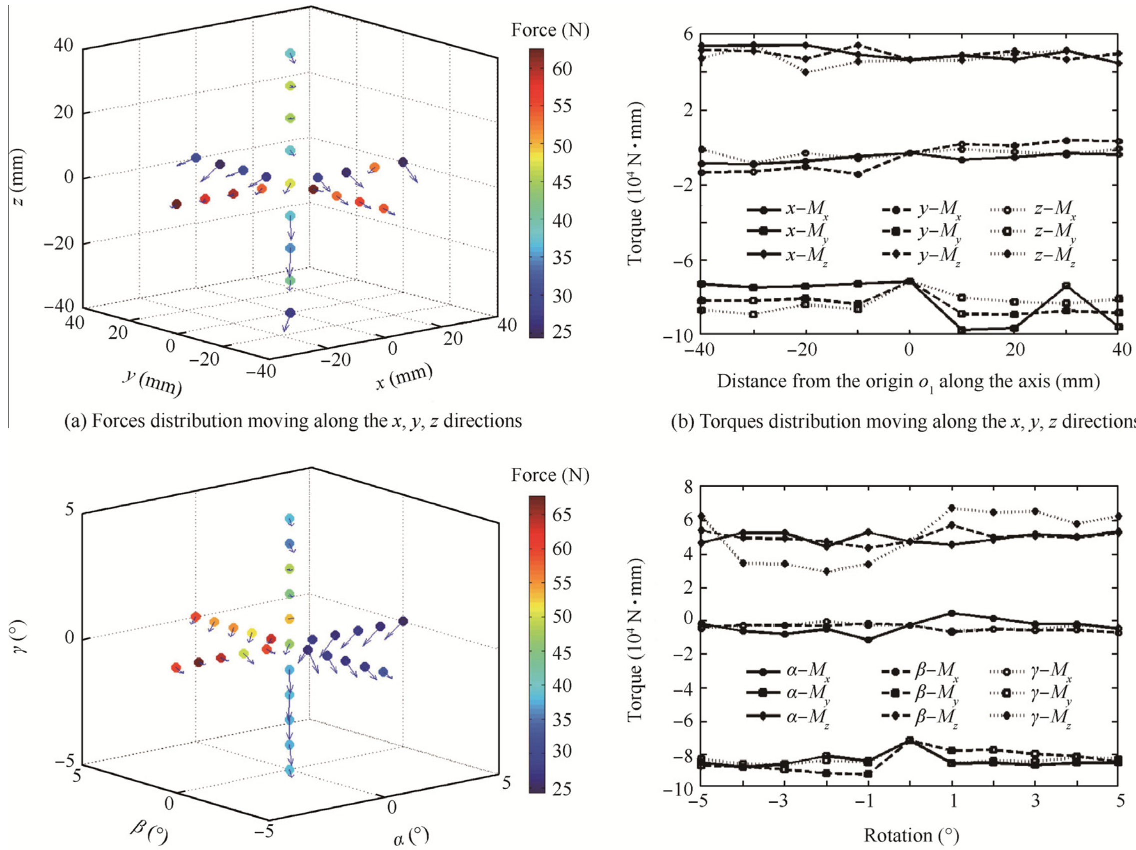

(a) Forces distribution moving along the x, y, z directions

(b) Torques distribution moving along the x, y, z directions

Fig. 9 Experimental results of measuring the six-dimensional F/T without assembly fixtures.

4.2.1. *Measuring the six-dimensional F/T without assembly fixtures*

The P&O adjusting platform without assembly fixtures is presented in Fig. 4. The P&O parameters of the moving platform were controlled for a motion of a single degree of freedom. Without assembly fixtures, the gravity value of the rigid system is 773.16 N (n = 18). The moving range in x, y, and z directions is ±40 with 10 mm variation for each measurement. The angle range is ±5° with 1° variation for each measurement. For every change in P&O parameters, 500 groups of the six-dimensional F/T were measured. The average F/T and relevant results are illustrated in Fig. 9.

Fig. 9(a) and (b) displays the F/T distribution of the P&O adjusting platform without assembly fixtures moving along the x, y, and z directions. Fig. 9(c) and (d) displays the F/T distribution of the P&O adjusting platform without assembly fixtures rotating around the x, y, and z directions. The location of the ball in Fig. 9(a) represents the control position, while in Fig. 9(c) the control orientation. The color bar on the right stands for the value of the measured force, with red areas being higher. The arrow of the ball shows the direction of the measured force. Fig. 9(b) and (d) presents the torque variations with respect to the pose parameters. Details about the black lines, markers, and line styles are listed in the legend.

From Fig. 9(a) and (c), it can be observed that when the P&O adjusting platform is moving along the x, y, and z directions without rotations, the deviations in the z direction are much smaller, compared to those in the other two directions. When the P&O adjusting platform is moving in the range of $x \geqslant 0$ or $y \geqslant 0$, the deviations are smaller, and the force magnitude accuracy A_{FM} is 30–35 N. The measured deviations increase when x decreases or y increases, and the biggest deviation is 60 N for $x = -40$ mm. When the P&O adjusting platform is rotating around the x, y, and z directions, the deviations around the z direction are much smaller, compared to those around the other two directions. The deviations are smaller for $\alpha \geqslant 0$ or $\beta \leqslant 0$, and the force magnitude accuracy A_{FM} is 30–35 N. The biggest deviation appears at $\alpha = -5°$ and its force magnitude accuracy A_{FM} is 65 N. The force vectors are all heading to the $-x$ and $-y$ directions, which indicates that a directional compensation could be made in the future to improve the accuracy of the algorithm.

From Fig. 9(b) and (d), it can be observed that when the P&O adjusting platform is moving along the x, y, and z directions without rotations, the torque accuracy A_{MX} shows enhanced compensation with smaller deviations. When the P&O adjusting platform without assembly fixtures is rotating around the x, y, and z directions, the torque accuracy A_{MX} shows enhanced compensation with smaller deviations.

4.2.2. *Measuring the six-dimensional F/T with assembly fixtures*

The P&O adjusting platform with assembly fixtures is presented in Fig. 10. The P&O parameters of the moving platform were controlled for a single degree of freedom of motion. Without assembly fixtures, the gravity value of the rigid system is 1912.09 N (n = 18). The moving range in the x, y, and z directions is ±30, with 10 mm variation for each measurement. The angle range is ±3° with 1° variation for each mea-

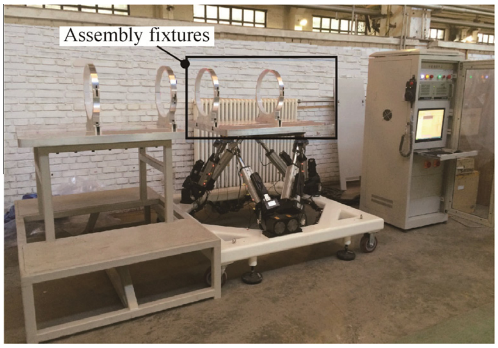

Fig. 10 P&O adjusting platform with assembly fixtures.

surement. For every change in P&O parameters, 500 groups of the six-dimensional F/T were measured. The average F/T and relevant results are illustrated in Fig. 11.

Fig. 11(a) and (b) displays the F/T distribution of the P&O adjusting platform with assembly fixtures moving along the x, y, and z directions, while Fig. 11(c) and (d) displays the F/T distribution of the P&O adjusting platform with assembly fixtures rotating around the x, y, and z directions. The location of the ball in Fig. 11(a) represents the control position, while in Fig. 11(c) the control orientation. The color bar on the right stands for the value of the measured force, with red areas being higher. The arrow of the ball shows the direction of the measured force. Fig. 11(b) and (d) shows the torque variations with respect to the pose parameters. Details about the black lines, markers, and line styles are listed in the legend.

From Fig. 11(a) and (c), it can be observed that when the P&O adjusting platform with assembly fixtures is moving along the x, y, and z directions without rotations, the deviations in the z direction are much smaller, compared to those in the other two directions. When the P&O adjusting platform is moving in the range of $x \geqslant 0$ or $y \geqslant 0$, the deviations are smaller, and the force magnitude accuracy A_{FM} is 30–55 N. The measured deviations increase when x decreases or y increases, and the highest deviation is 80 N for $y = -15$ mm. When the P&O adjusting platform is rotating around the x, y, and z directions, the deviations around the z direction are much smaller, compared to those of the other two directions. The deviations are smaller for $\alpha \geqslant 0$ or $\beta \leqslant 0$, and the force magnitude accuracy A_{FM} is 30–55 N. The biggest deviation appears at $\alpha = -3°$ and its force magnitude accuracy A_{FM} is 65 N. The force vectors are all heading to the $-x$ and $-y$ directions, which indicate that a directional compensation could be made in the future to improve the algorithm's accuracy.

From Fig. 11(b) and (d), it can be observed that when the P&O adjusting platform is moving along the x, y, and z directions without rotations, the torque accuracy A_{MX} shows enhanced compensation with small deviations. When the P&O adjusting platform with assembly fixtures is rotating

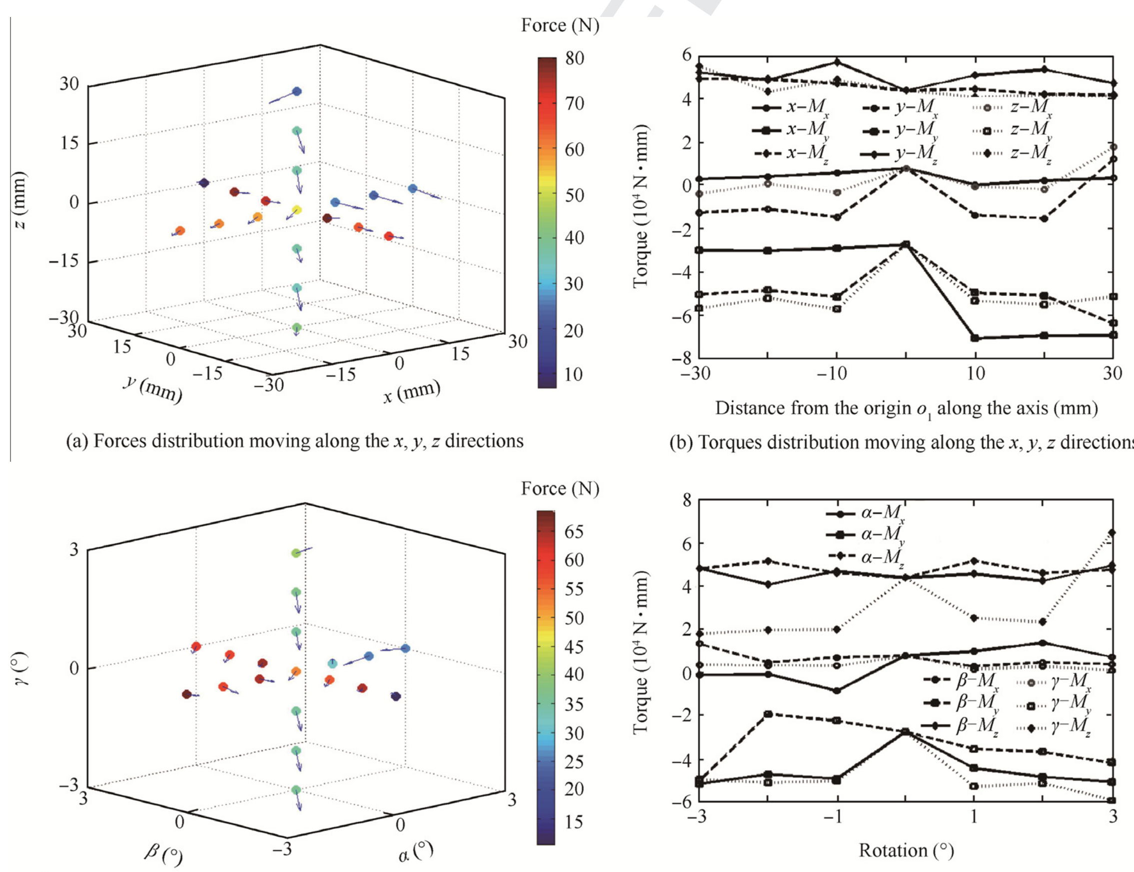

(a) Forces distribution moving along the x, y, z directions

(b) Torques distribution moving along the x, y, z directions

(c) Forces distribution rotating around the x, y, z directions

(d) Torques distribution rotating around the x, y, z directions

Fig. 11 Experimental results of measuring the six-dimensional F/T with assembly fixtures.

Please cite this article in press as: Wen K et al. Algorithm and experiments of six-dimensional force/torque dynamic measurements based on a Stewart platform, *Chin J Aeronaut* (2016), http://dx.doi.org/10.1016/j.cja.2016.10.015

around the x, y, and z directions, the torque accuracy A_{MX} shows enhanced compensation with small deviations as well.

Comparisons between Sections 4.1 and 4.2 lead to the conclusion that the measurement accuracy of the six dimensional F/T is different under different P&O sets. Therefore, a preferable operation range of the P&O adjusting platform can be selected for high-precision assembly with smaller deviations. The accuracy of measuring the six-dimensional F/T with assembly fixtures is inferior to that observed without assembly fixtures, and the deviations are higher. This is attributed to the weight difference between the assembly fixtures and the moving platform. In this case, the assembly fixtures are twice as heavy as the moving platform, which lowers the accuracy of dynamic gravity compensation as well as the coupling effect of the six-dimensional F/T in the analytical algorithm.

4.3. *F/T-driven alignment of large components*

Experiments of the F/T-driven alignment for large components were performed on the designed digital flexible alignment system using aerospace products (as in Fig. 12), and the alignment process can be described by the flowchart shown in Fig. 13. Firstly, according to the precision analysis results of Section 4.2, the threshold value of the six-dimensional F/T could be obtained. In the experiment, the threshold value of the force magnitude was 60 N, and the threshold value of the torque magnitude was 25 N·m. Secondly, an operator judged the direction of the applied force by visual, and then an external force was applied to the P&O adjusting platform by the operator. Thirdly, the six-dimensional F/T was calculated in real time by dynamic gravity compensation. Fourthly, intention recognition methods were designed through the threshold value, the direction and magnitude of the force, and the torque. In the end, the P&O adjusting platform adjusted the P&O of the large component to follow the intentions of the operator.

In the above experiments, the alignment process was completed successfully. The experimental results proved that the precision analysis of the six-dimensional F/T was correct and effective, and the intention recognition was correct. The alignment process met the real-time requirements. The analytical algorithm and precision analysis of the six-dimensional F/T based on the P&O adjusting platform laid the foundation for F/T-driven alignment of large components.

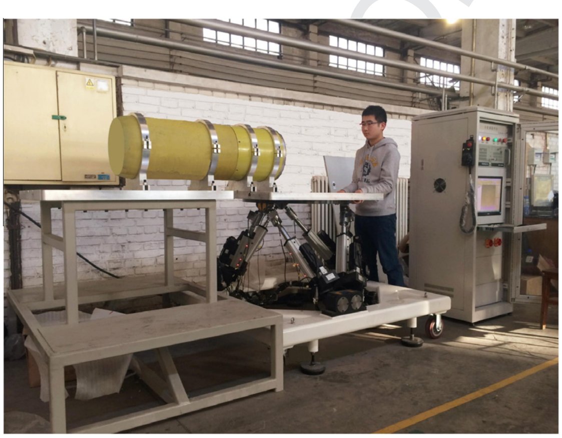

Fig. 12 Alignment system of large components for F/T-driven assembly.

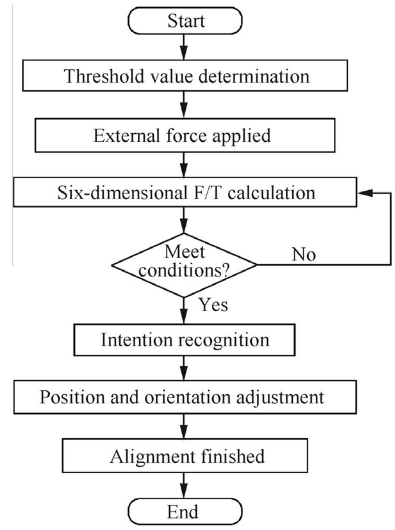

Fig. 13 Flowchart of the F/T-driven alignment.

5. Conclusions

The P&O adjusting platform can dynamically measure interactive forces. This paper provides an analytical algorithm of the interaction forces between components and takes into consideration dynamic gravity deviations as influential factors. The relevant experimental results show that the proposed analytical algorithm can evaluate gravity deviations and make reliable compensations. The contributions of the paper are summarized as follows:

(1) An analytical algorithm of the six-dimensional F/T based on the screw theory is proposed for accurate determination of external forces during high-precision alignment. Dynamic gravity deviations are taken into consideration and a precise compensation model is provided. Barycenter coordinates and gravity directions are discussed in details. Meanwhile, the choice of the P&O number is optimized for a stable and efficient compensation through experiments.
(2) An approximation cone shape is used for spatial precision analysis. Given the specific appearance of the repeated six-dimensional F/T measurements, the magnitudes and directions of the measured F/T could be evaluated by a set of standards, regarding accuracy and repeatability.
(3) Known applied load measurement experiments have been performed on the P&O adjusting platform based on an SP for F/T-driven alignment, and relevant experimental data adequately prove that the proposed analytical algorithm could accurately predict the F/T with small deviations. Precision analysis experiments have been performed on the P&O adjusting platform (without or with assembly fixtures), and relevant experimental data adequately prove that the measurement accuracy of the six-dimensional F/T is different under different P&O sets. Higher loads lead to poorer accuracy of

Please cite this article in press as: Wen K et al. Algorithm and experiments of six-dimensional force/torque dynamic measurements based on a Stewart platform, *Chin J Aeronaut* (2016), http://dx.doi.org/10.1016/j.cja.2016.10.015

dynamic gravity compensation. In addition, the preferable operation range is discussed for high-precision alignment with smaller deviations. Based on the above analysis, the experiments of F/T-driven alignment for large components have been completed successfully.

(4) Interactive force measurements are novel and significant for high-precision assembly, and the present algorithm could fulfill accurate force determination and provide satisfactory dynamic gravity compensation. Measuring the six-dimensional F/T could be further improved with higher motion control of the moving platform or more accurate measurements of forces or limb lengths. Besides, the coupling effect for the P&O parameters, varying in synchronization and force control techniques, should be studied in future research.

Acknowledgments

This study was co-supported by the National Defense Basic Scientific Research (No. A2120132007) and the Fund of National Engineering and Research Center for Commercial Aircraft Manufacturing (No. SAMC14-JS-15-055).

Appendix A. Supplementary material

Supplementary data associated with this article can be found, in the online version, at http://dx.doi.org/10.1016/j.cja.2016.10.015.

References

1. Mei ZY, Maropoulos PG. Review of the application of flexible, measurement-assisted assembly technology in aircraft manufacturing. *Proc IME B J Eng Manuf* 2014;**228**(10):1185–97.
2. Chen ZH, Du FZ, Tang XQ. Research on uncertainty in measurement assisted alignment in aircraft assembly. *Chin J Aeronaut* 2013;**26**(6):1568–76.
3. Yao R, Zhu WB, Huang P. Accuracy analysis of Stewart platform based on interval analysis method. *Chin J Mech Eng* 2013;**26**(1):29–34.
4. Rosenzveig V, Briot S, Martinet P, Ozgur E, Bouton N. A method for simplifying the analysis of leg-based visual servoing of parallel robots*IEEE international conference on robotics & automation (ICRA), May 31-June 7, Hong Kong, China.*
5. Pedrammehr S, Mahboubkhah M, Khani N. A study on vibration of Stewart platform-based machine tool table. *Int J Adv Manuf Technol* 2013;**65**(5):991–1007.
6. Denkenaa B, Holza C, Abdellatifb H. Model-based control of a hexapod with linear direct drives. *Int J Comput Integr Manuf* 2006;**19**(5):463–72.
7. Dalvand MM, Shirinzadeh B. Motion control analysis of a parallel robot assisted minimally invasive surgery/microsurgery system (PRAMiSS). *Robot Comput-Int Manuf* 2013;**29**(2):318–27.
8. Tang F. Development of an engineering simulator for armored vehicle*International conference on automation, mechanical control and computational engineering, Apr 24–26, Jinan, China.*
9. Pisla A, Itul T, Pisla D, Szilaghyi A. Considerations upon the influence of manufacturing and assembly errors on the kinematic and dynamic behavior in a flight simulator Stewart-Gough platform. *Mech, Transm Appl: Mech Mach Sci* 2012;**3**:215–23.
10. Lochte C, Dietrich F, Raatz A. A parallel kinematic concept targeting at more accurate assembly of aircraft sections. *Intell Robot Appl* 2011;**7101**:142–51.
11. Xu YF, Yuan JR, Zhao J, Zhao YB. Robust attitude control and simulation of a Stewart spacecraft*The 27th Chinese control and decision conference, May 23–25, Qingdao, China.*
12. Zhao H, Zhang SY, Chen XD. Compliant force control in space docking*Proceedings of the 2007 IEEE international conference on mechatronics and automation, Aug 5–8, Harbin, China.*
13. Zhang GQ, Du JJ, To S. Calibration of a small size hexapod machine tool using coordinate measuring machine. *Proc IME E J Process Mech Eng* 2014.
14. Zhou WY, Chen WY, Liu HD. A new forward kinematic algorithm for a general Stewart platform. *Mech Mach Theory* 2015;**87**:177–90.
15. Jamshidi J, Kayani A, Iravani P, Summers MD. Manufacturing and assembly automation by integrated metrology systems for aircraft wing fabrication. *Proc IME B J Eng Manuf* 2010;**224**(1):25–36.
16. Chen ZH, Du FZ, Tang XQ, Zhang X. A framework of measurement assisted assembly for wing-fuselage alignment based on key measurement characteristics. *Int J Manuf Res* 2015;**10**(2):107–28.
17. Zheng LY, Zhu XS, Liu RW, Wang YW, Maropoulos PG. A novel algorithm of posture best fit based on key characteristics for large components assembly. *Procedia CIRP* 2013;**10**:162–8.
18. Galetto M, Mastrogiacomo L. Analysing uncertainty contributions in dimensional measurements of large-size objects by ultrasound sensors. *Int J Comput Integr Manuf* 2014;**27**(1):36–47.
19. Ferria C, Mastrogiacomob L, Farawayc J. Sources of variability in the set-up of an indoor GPS. *Int J Comput Integr Manuf* 2010;**23**(6):487–99.
20. Muelaner JE, Cai B, Maropoulos PG. Large-volume metrology instrument selection and measurability analysis. *Proc IME B J Eng Manuf* 2010;**224**(6):853–68.
21. Yao JT, Zhang HY, Zhu JL, Xu YD, Zhao YS. Isotropy analysis of redundant parallel six-axis force sensor. *Mech Mach Theory* 2015;**91**:135–50.
22. Yao JT, Li WJ, Zhang HY, Xu YD, Zhao YS. Task-oriented design method and experimental research of six-component force Sensor. *Intell Robot Appl* 2014;**8917**:1–12.
23. Dwarakanath TA, Bhutani G. Beam type hexapod structure based six component force-torque sensor. *Mechatronics* 2011;**21**(8):1279–87.
24. Liu W, Li Q, Jia ZY, Jiang E. Design and experiment of a parallel six-axis heavy force sensor based on Stewart structure. *Sensors Transd* 2013;**151**(4):54–62.
25. Kim YL, Song HC, Song JB. Hole detection algorithm for chamferless square peg-in-hole based on shape recognition using F/T sensor. *Int J Prec End Manuf* 2014;**15**:425–32.
26. Jasim IF, Plapper PW. Contact-state monitoring of force-guided robotic assembly tasks using expectation maximization-based Gaussian mixtures models. *Int J Adv Manuf Technol* 2014;**73**(5):623–33.
27. Shirinzadeh B, Zhong Y, Tilakaratna PDW, Tian YL, Dalvand MM. A hybrid contact state analysis methodology for robotic-based adjustment of cylindrical pair. *Int J Adv Manuf Technol* 2011;**52**(1):329–42.
28. Park DI, Park C, Do H, Choi T, Kyung JH. Assembly phase estimation in the square peg assembly process*The 12th international conference on control, automation and systems, Oct 17–21, JeJu Island, Korea.*
29. Wiemer SC, Schimmels JM. Optimal admittance characteristics for planar force-assembly of convex polygonal parts*2012 IEEE international conference on robotics and automation, May 14–18, Saint Paul, MN, USA.*
30. Bera TK, Merzouki R, Bouamama BO, Samantaray AK. Force control in a parallel manipulator through virtual foundations. *Proc IME I J Syst Control Eng* 2012;**226**(8):1088–106.

31. Qiao H, Dalay BS, Parkin RM. Robotic peg-hole insertion operations using a six-dimensional force sensor. *Proc IME C J Mech Eng Sci* 1993;**207**:289–305.
32. Geng MC, Zhao TS, Wang C, et al. The study of the direct position analysis of parallel mechanism based on quasi-newton method. *J Mech Eng* 2015;**51**(9):28–36 [in Chinese].

Wen Ke is a Ph.D. student in the School of Mechanical Engineering and Automation at Beihang University. His area of research includes measurement-assisted assembly technologies research and applications.

Du Fuzhou is an associate professor and M.S. advisor in the School of Mechanical Engineering and Automation at Beihang University. His main research interests are measurement-assisted assembly, quality management, and quality engineering.

Zhang Xianzhi is an instructor and Ph.D. advisor in the School of Mechanical and Aerospace Engineering at Kingston University in U.K. His current research interests are CAM, STEP-NC, and manufacturing informatics.